Cell. Mol. Life Sci. (2010) 67:3711–3723
DOI 10.1007/s00018-010-0398-3

Cellular and Molecular Life Sciences

RESEARCH ARTICLE

Differentiating effects of the glucagon-like peptide-1 analogue exendin-4 in a human neuronal cell model

Paola Luciani · Cristiana Deledda · Susanna Benvenuti · Ilaria Cellai · Roberta Squecco · Monica Monici · Francesca Cialdai · Giorgia Luciani · Giovanna Danza · Chiara Di Stefano · Fabio Francini · Alessandro Peri

Received: 26 January 2010 / Revised: 31 March 2010 / Accepted: 30 April 2010 / Published online: 23 May 2010

Abstract Glucagon-like peptide-1 (GLP-1) is an insulinotropic peptide with neurotrophic properties, as assessed in animal cell models. Exendin-4, a GLP-1 analogue, has been recently approved for the treatment of type 2 diabetes mellitus. The aim of this study was to morphologically, structurally, and functionally characterize the differentiating actions of exendin-4 using a human neuronal cell model (i.e., SH-SY5Y cells). We found that exendin-4 increased the number of neurites paralleled by dramatic changes in intracellular actin and tubulin distribution. Electrophysiological analyses showed an increase in cell membrane surface and in stretch-activated-channels sensitivity, an increased conductance of Na^{+} channels and amplitude of Ca^{++} currents (T- and L-type), typical of a more mature neuronal phenotype. To our knowledge, this is the first demonstration that exendin-4 promotes neuronal differentiation in human cells. Noteworthy, our data support the claimed favorable role of exendin-4 against diabetic neuropathy as well as against different neurodegenerative diseases.

Keywords Diabetic neuropathy · GLP-1 · Neuritogenesis · Neuroprotection · Exendin-4

P. Luciani · C. Deledda · S. Benvenuti · I. Cellai · G. Danza · C. Di Stefano · A. Peri
Endocrine Unit, Department of Clinical Physiopathology, Center for Research, Transfer and High Education on Chronic, Inflammatory, Degenerative and Neoplastic Disorders for the Development of Novel Therapies (DENOThe), University of Florence, Florence, Italy

M. Monici · F. Cialdai
Joint Laboratory ASAcampus, ASA Research Division, Department of Clinical Physiopathology, University of Florence, Florence, Italy

R. Squecco · G. Luciani · F. Francini
Department of Physiological Sciences, University of Florence, Florence, Italy

A. Peri (✉)
Endocrine Unit, Department of Clinical Physiopathology, University of Florence, Viale Pieraccini, 6, 50139 Florence, Italy
e-mail: a.peri@dfc.unifi.it

Introduction

Glucagon-like peptide-1 (GLP-1) is a post-translational cleavage product of the *proglucagon* gene by the pro-hormone convertase PC1/3 [1, 2]. This peptide is mainly produced in enteroendocrine L-cells in response to nutrient ingestion [3, 4] and its most studied effect is related to the stimulatory action on insulin secretion by pancreatic β-cells together with the inhibition of gastric emptying [5] and glucagon secretion [6]. However, GLP-1 use as a therapeutic agent for the treatment of type 2 diabetes mellitus (T2DM) is impractical because of its extremely short half-life (1.5 min in rodents and humans) [7]. Exendin-4 is a more stable GLP-1 analog, with a half-life of approximately 4 h in humans [8]. Its synthetic form (i.e., exenatide) was approved by the US Food and Drug Administration in April 2005 as an adjunctive therapy to metformin, a sulfonylurea or a thiazolidinedione for the treatment of T2DM. GLP-1 and exendin-4 bind and activate the GLP-1 receptor (GLP-1R), a G protein-coupled receptor that increases intracellular cAMP levels by activating transmembrane adenylate cyclase [9–11]. Receptors are located in various tissues including heart, kidney, lungs [12], and brain, where they are particularly abundant in the paraventricular and arcuate nucleus, and in the hypothalamus, which are key brain regions involved in feeding control [13]. Studies performed in rodents indicated that GLP-1R agonists reduce short-term food intake when injected either

peripherally or into the central nervous system (CNS), and their repeated injection significantly inhibits not only food intake but also weight gain [14–18]. Moreover, the thalamus, brainstem, lateral septum, subfornical organ, area postrema, cerebral cortex, cerebellum, caudate-putamen, and hippocampus express GLP-1R, thus suggesting that GLP-1 may have further effects in the CNS [19, 20]. As a matter of fact, GLP-1R-knock-out mice present for instance reduced learning abilities and are more susceptible to kainic acid-induced seizures and neuronal degeneration in the hippocampus than wild-type mice [21]. Neuroprotective effects of GLP-1 and exendin-4 have been investigated in several studies. In cultured rat hippocampal neurons expressing functional GLP-1R, GLP-1 and exendin-4 effectively protect against glutamate-induced cell death [22] and against Aβ- and iron-induced apoptosis [23]. Another study demonstrated that the administration of exendin-4 reduces brain damage and improves functional outcome in a transient middle cerebral artery occlusion stroke model [24]. In the same study it was also shown that exendin-4 treatment protects dopaminergic neurons against degeneration, preserves dopamine levels, and improves motor function in a mouse model of Parkinson's disease [24]. The evidence of the neurotrophic role of GLP-1R agonists has been further supported by the demonstration of a differentiating effect of GLP-1 and exendin-4 on rat pheochromocytoma cells (PC12). In this model, both molecules were able to induce neurite outgrowth and expression of neuronal markers similar to those induced by nerve growth factor (NGF) [25]. Despite the encouraging data obtained both in vivo and in vitro on animal models, to date no study has yet thoroughly assessed the activity of GLP-1R agonists on human neuronal cells. Therefore, the aim of this study was to extensively investigate for the first time in a human neuronal cell model the role of exendin-4 in promoting neuronal differentiation. To this purpose, SH-SY5Y neuroblastoma cells were used as the cell model. These cells are commercially available, can be readily propagated in vitro, and represent a well-established model for the assessment of cell differentiation [26, 27].

Materials and methods

Cells and treatments

The human neuroblastoma cell line SH-SY5Y (American Type Culture Collection, Manassas, VA, USA) was cultured in RPMI medium supplemented with 10% FBS, 200 mM L-glutamine, 100 IU/ml penicillin, 100 μg/ml streptomycin and maintained at 37°C in a humidified atmosphere (5% CO_2/95% air). All the reagents for cell cultures, LY294002 and U0126 were from Sigma Chemical Co. (St. Louis, MO, USA). Tissue plastic-ware was from Bibby Sterilin (Staffordshire, UK). The cells were seeded in six-well plates, maintained in low serum conditions (RPMI medium supplemented with 2% FBS), and treated with exendin-4 (300 nM) or with all-trans retinoic acid (10 μM) (Sigma) for 24 and 48 h.

Real-time RT-PCR and intracellular cAMP determination

The quantification of GLP-1 receptor, RhoA and Rho-activated kinase 1 (ROCK1) mRNA was performed by real-time RT-PCR based on TaqMan technologies. Primers and probe for human GLP-1R were R: 5′-GGCCAG CAGGCGTATTCA-3′ F: 5′-CCTCCTGCCACAGAC TTGTTC-3′ probe: 5′ FAM-CAACCGGACCTT CG-TAM RA 3′. The mRNA amount of Rho A and ROCK1 genes was quantified using the Applied Biosystems TaqMan Gene Expression assays (number Hs00357608_m1 and Hs00178463_m1, respectively). Each measurement was carried out in triplicate. The mRNA quantitation was based on the comparative Ct (for cycle threshold) method. Data were normalized to ribosomal 18S RNA expression and reported as $2^{-\Delta\Delta Ct}$ [28].

Intracellular cyclic AMP was measured using cAMP-direct Immuno Assay KIT (Calbiochem) according to the manufacturer's instructions. Triplicate SH-SY5Y cell cultures were treated with 300-nM exendin-4 in the presence of 0.5 mM isobutylmethylxanthine (IBMX) and harvested at 2-min intervals after the onset of treatment for a total period of 30 min. The cAMP concentrations were calculated on a standard curve generated using serial dilution of cAMP Standard solution.

Quantification of neurite outgrowth and treatments with signaling pathway inhibitors

SH-SY5Y cells, cultured in low serum media as described above were maintained in control conditions or treated with exendin-4 0.3 μM or RA 10 μM for 24, 48 and 72 h. Using phase-contrast microscopy, we evaluated ten random fields of cells in order to quantify the number of neurites. The length of the neurites was measured by the means of the AxioVision Zeiss program (Zeiss Gottingen, Germany). Three independent operators scored a total amount of 100 cells per treatment. For treatments with signaling pathway inhibitors, a 20-mM stock solution each of LY294002 and U0126 were prepared in dimethylsulfoxide, stored at −20°C and diluted with medium just before use; the final concentrations were 10 μM LY294002 and 5 μM U0126. Cells were exposed to inhibitors with or without exendin-4 (0.3 μM) for 48 h before neurite evaluation. Data represent the mean ± SE of three independent experiments.

Cell viability assays

Cell viability following exposure to 300-nM exendin-4 and/or 20 and 50 μM H_2O_2 was determined by MTS assay (Promega Corporation, Madison, WI, USA) and Trypan Blue dye exclusion test, as described previously [29]. The results were expressed as mean ± SE of three different experiments.

Immunofluorescence microscopy

After the treatments, the cells were fixed for 5 min in cold acetone and then washed in PBS. After blocking unspecific binding with PBS containing 3% BSA, the cells were incubated overnight at 4°C with the specific anti-human monoclonal antibodies anti-tubulin, actin) (Chemicon). The cells were then incubated with anti-mouse IgG FITC (fluorescein isothiocyanate) conjugated (Chemicon). Negative controls were obtained by omitting the primary antibodies. Samples were evaluated by an epifluorescence microscope (Nikon) at 100× magnification and imaged by a HiRes IV digital CCD camera (DTA). Image analysis was performed by extracting, for each cell image, the region of interest (ROI) by appropriate software (Image-Pro Plus). All the experiments were carried out in triplicate. For immunofluorescence analysis, at least 30 cells per slide were scored in ten random fields/slide. Fluorescence semi-quantitative evaluation of the distribution of tubulin was performed by three different operators for at least ten fields.

Apoptosis

Apoptosis was evaluated by TUNEL analysis, using the ApopTag® Fluorescein In Situ Apoptosis Detection Kit purchased from Chemicon International. Cells were seeded in coverslips and incubated in the presence or absence of exendin-4 and H_2O_2 (20 and 50 μM) for 3 h. Samples were processed following the manufacturer's instructions.

Western-blot analysis

Samples were kept in lysis buffer [20 mM Tris–HCl, 150 mM NaCl, 0.2 mM EDTA, 0.3% Triton X-100, 1 mM Na_3VO_4, 1 mM phenylmethylsulfonyl fluoride, 1 μg/ml leupeptin], supplemented with Complete Protease Inhibitor Cocktail (Roche Applied Science, Milan, Italy) for 2 h at 0°C. Protein concentration was measured using a Coomassie Bio-Rad protein assay kit (Bio-Rad, Hercules, CA, USA). SDS-PAGE and Western-blot analysis were performed as described previously [30]. The blots obtained were incubated with anti-Phospho-Cofilin and anti-Cofilin antibodies (Cell Signaling). The intensities of the immunoreactive bands were quantified by means of Quantity One software on a ChemiDoc XRS instrument (Bio-Rad Labs, Hercules, CA). Each band was normalized with respect to its corresponding signal stained with GAPDH (glyceraldehyde 3-phosphate dehydrogenase) antibody (Sigma). Results are mean ± SE of three experiments.

Electrophysiology

Patch pipettes (3–7 MΩ) made from borosilicate glass tubing (Harvard Apparatus LTD) using a vertical puller (Narishige, Tokyo, Japan) were used for whole-cell current- and voltage-clamp recordings. Recording pipettes were filled with a solution that contained (mM): 150 CsBr, 5 $MgCl_2$, 10 EGTA, and 10 HEPES, pH 7.2, with KOH. Coverslips with the adherent cells (control SH-SY5Y neuroblasts and exendin-4, EXE,- or retinoic acid, RA,-treated for 48 h SH-SY5Y) were superfused at a rate of 1.8 ml min^{-1} with a physiological bath solution (mM): 150 NaCl, 5 KCl, 2.5 $CaCl_2$, 1 $MgCl_2$, 10 D-glucose and 10 HEPES, pH 7.4 with NaOH. To test the voltage-activated Na^+ channel activity, we used TTX (1 μM). When outward K^+ currents had to be suppressed, experiments were performed in a 20 mM-TEA bath solution (mM): 122.5 NaCl, 2 $CaCl_2$, 20 TEA-OH, and 10 HEPES. Ca^{2+} currents were recorded in a Na^+- and K^+-free solution, TEA-Ca^{2+} bath solution, contained (mM): 10 $CaCl_2$, 145 TEABr, and 10 HEPES. Nifedipine (10 μM) was used to avoid the occurrence of the (HVAC) L-type Ca^+ currents and Cd^{2+} (0.8 mM) to block all high-voltage-activated channels, HVACs, as L- and N-type Ca^{2+} current. The whole-cell configuration was obtained after gentle application of negative pressure. Access resistance was continuously monitored during the experiments. Only those cells in which access resistance (changes < 10%) was stable were included in the analysis. Pclamp6 (Axon Instruments, Foster City, CA) software was used for analysis. The technique, setup, and electronics are as described in detail previously [28, 31]. Stretch-activated channel, SAC, sensitivity was evaluated as reported in Formigli et al. [32]. To inactivate mostly of I_{Na} and I_{Ca} the holding potential of −40 mV and a pulse protocol (100 ms long) ranging from −80 to 0 mV in 10-mV increments were applied from a pre-step to −60 mV. The resting membrane potentials (RMP) were recorded by switching to the current clamp mode of the 200 B amplifier. Experiments were performed at 22°C.

Statistical analysis

Results from multiple experiments are expressed as mean ± SEM. Significance of differences between means was tested using Student's t test. Values of $p < 0.05$ were

considered statistically significant. For multiple comparisons, one-way ANOVA with repeated measures was utilized.

Results

SH-SY5Y cells express a functional GLP-1R

The presence of GLP-1R was detected in SH-SY5Y neuroblastoma cells by real-time RT-PCR analysis ($2^{-\Delta\Delta Ct} \times 10^4 = 2.24 \pm 0.015$, mean $\pm$ SE). In order to evaluate the functionality of the GLP-1R, a time-course analysis of its activation was performed. Exendin-4 has been shown to stimulate adenylyl cyclase, leading to an increase in intracellular cAMP [9]. cAMP was assayed at 2-min intervals after treatment with 300 nM exendin-4 (Fig. 1). There was a maximal five-fold increase in cAMP levels within 4 min after stimulation. These findings demonstrate the presence of a functionally active GLP-1R on SH-SY5Y cells.

Exendin-4 induces differentiation of SH-SY5Y cells

SH-SY5Y cells were maintained in low serum conditions or exposed to 300 nM exendin-4. Figure 2a shows a representative experiment in which the neurite sprouting induced by exendin-4 is compared to that induced by retinoic acid (RA), the classical neuronal differentiating agent for these cells [33], which was used as the control. Daily quantification of neuritic development was carried out. In Fig. 2b, the percentage of cells with neurites after 24–48–72 h of treatment is reported. Both RA and exendin-4 treatment significantly increased the number of cells bearing neurites, whereas the combined treatment with RA and exendin-4 did not produce additive effects. Exendin-4- and RA-mediated morphological changes display different characteristics, as indicated by the fact that the number of

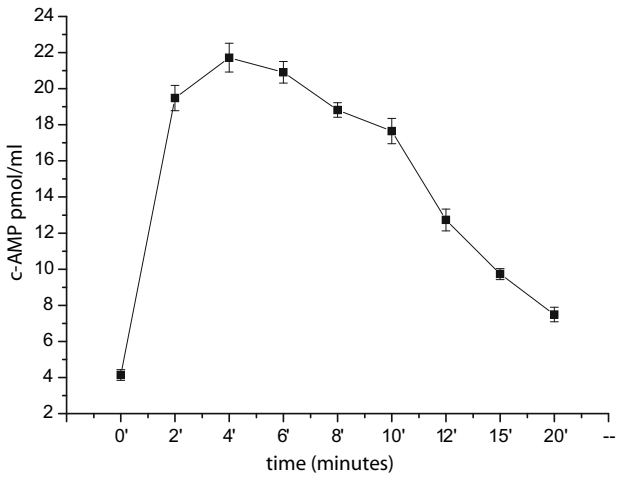

Fig. 1 Intracellular cAMP determination after incubation with exendin-4 at different time points. *Vertical error bars* represent ±SE of three independent experimental values

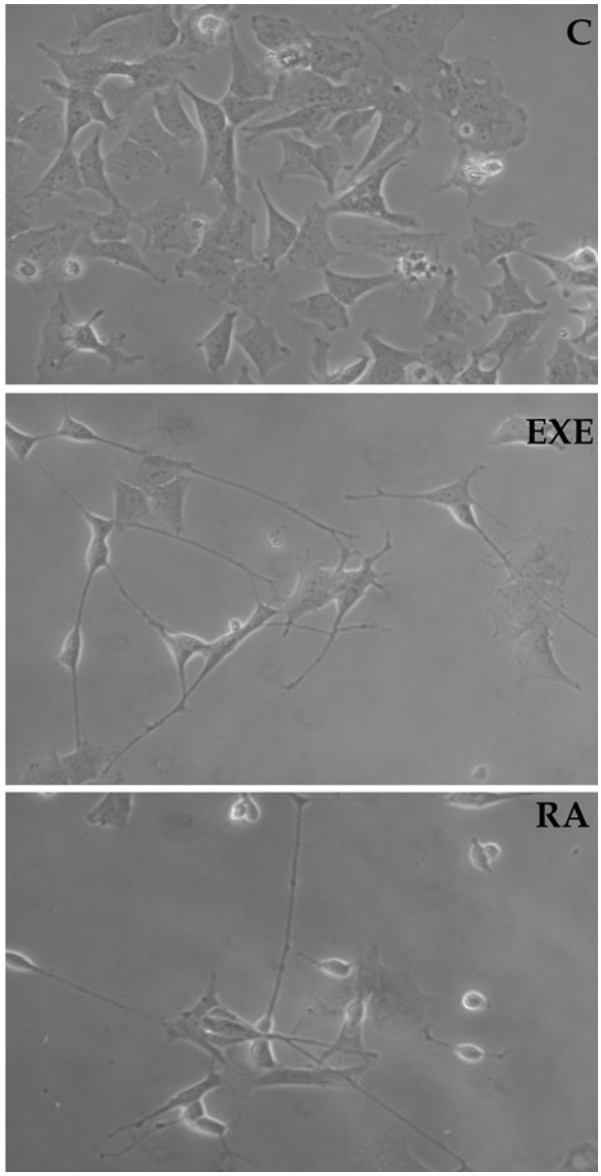

Fig. 2 **a** Phase-contrast inverted microscopy (40× magnification) pictures showing the morphology of SH-SY5Y cells before (C) and after 48-h treatment with exendin-4 (EXE) or with the differentiation positive control RA. **b–d** Analysis of the morphological changes induced by exendin-4 (EXE) (*black bars*), RA (*grey bars*) or EXE + RA (*sparse pattern bars*) compared to untreated cells (C, *white bars*) evaluated at different times (24, 48, and 72 h); **b** Percentage of cells bearing neurites; **c** number of neurites per cell; **d** Neurite length (μm) * = $p < 0.05$ versus C; # = $p < 0.05$ versus exendin-4, one-way ANOVA test. **e** Effects of specific signaling inhibitors on EXE-induced differentiation: percentage of cells bearing neurites after exposure to EXE with or without the PI-3 K inhibitor LY294002 or the MAPK/ERK kinase inhibitor U0126. * = $p < 0.05$ versus C; § = $p < 0.05$ versus EXE, Student's *t* test

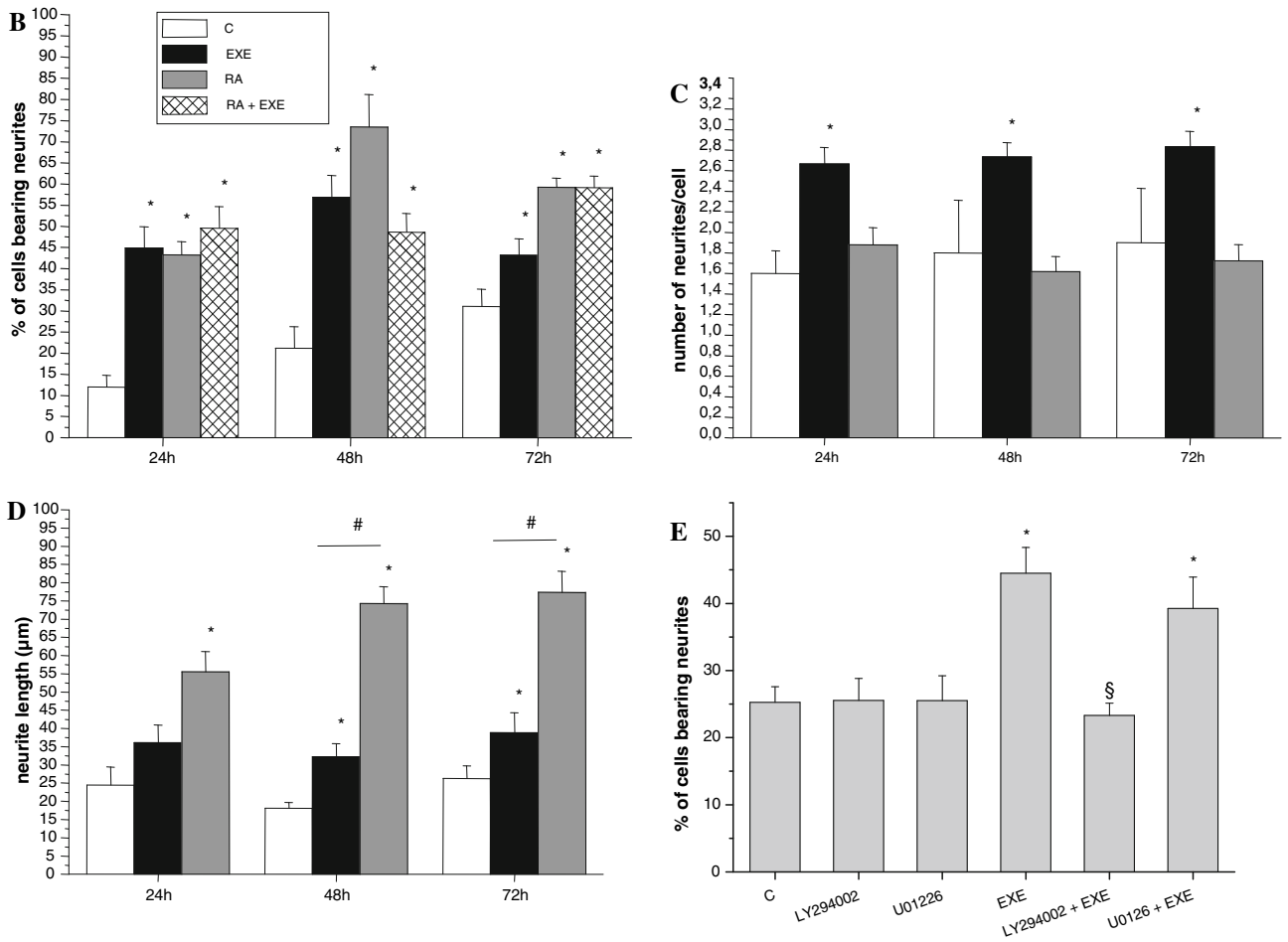

Fig. 2 continued

neurites/cell was significantly higher only after exendin-4 treatment, as is shown in Fig. 2c. Moreover, the length of neurites induced by exendin-4 was markedly shorter than that of neurites induced by RA, as is reported in Fig. 2d. Overall, these data suggest that exendin-4 may induce differentiation in SH-SY5Y cells by affecting the number of the neurites rather than their length.

We subsequently evaluated the expression of two members of the Rho-GTPase family, which are known regulators of neuronal development [34], by quantitative real-time RT-PCR. We found that RhoA expression was significantly reduced both by exendin-4 and RA [0.4 ± 0.031 and 0.56 ± 0.025, respectively (mean $\pm$ SE), versus untreated cells taken as 1, $p < 0.05$]. A significant reduction was also observed for ROCK1 expression [0.54 ± 0.05 and 0.57 ± 0.02, respectively (mean $\pm$ SE), versus untreated cells taken as 1, $p < 0.05$].

To evaluate the possible pathways involved in exendin-4-induced differentiation, we quantified the number of cells with neurites using the phosphatidylinositol 3-kinase (PI3-K) inhibitor LY294002, and the mitogen-activated protein kinase (MAPK)/extracellular signal-regulated kinase (ERK) inhibitor U0126. It is known that both the PI3-K and the MAPK/ERK pathways are involved in GLP-1R-mediated differentiation of pancreatic β cells [35] and the latter has been associated with neuronal differentiation of neuronal-derived PC12 cells [36]. Neither LY294002 nor U0126 altered cell viability in MTS assays (data not shown), as already reported in SH-SY5Y cells [37, 38]. The MAPK/ERK inhibitor did not affect neurite outgrowth, whereas the PI3-K inhibitor LY294002 completely abolished the differentative process (Fig. 2e), thus suggesting a role of PI3-K in exendin-4-induced neuritogenesis in this cell model.

Analysis of cytoskeletal actin and tubulin

Neuronal differentiation is accompanied by profound morphological alterations, including the elaboration of dendritic and axonal neurites. The relative requirement for plasticity in outgrowing neurites versus stabilized axons is reflected by their cytoskeletal composition. The very first

morphogenetic event in neurite initiation involves reorganization of both microtubules and filamentous actin. Therefore, in order to assess the effect of exendin-4 on neuronal differentiation, we analyzed by immunofluorescence microscopy the expression of the cytoskeleton proteins tubulin and actin, which form microtubules and microfilaments, respectively (Fig. 3). In a and d, the distribution of actin and tubulin, respectively, in untreated cells is shown. Exendin-4 treatment significantly increased filamentous (F) -actin accumulation and the formation of cone-like structures (Fig. 3b), whereas RA induced a weaker modification in actin polymerization (Fig. 3c). Transcytoplasmatic stress fibers, long and parallel filaments which crossed the cell from end to end, strongly increased in cells treated with exendin-4. Tubulin analysis revealed the accumulation of microtubules into the neurites both after exendin-4 and RA treatment (Fig. 3e, f); however, the effect was more evident in exendin-4-treated cells, as assessed by a semi-quantitative evaluation of the distribution and intensity of tubulin (Fig. 3g). These observations suggest a coordinated polymerization of actin and tubulin induced by exendin-4, aiming to favor neurite formation in SH-SY5Y cells.

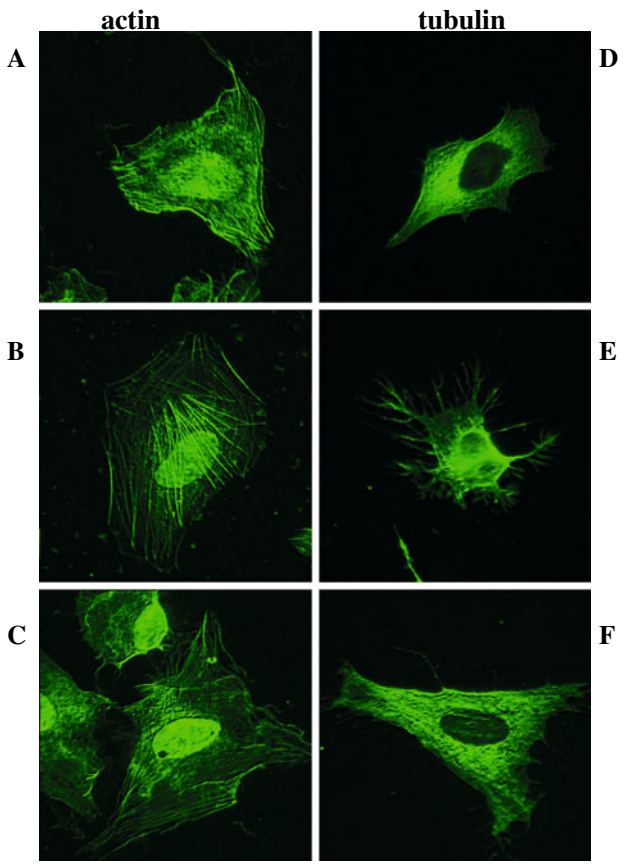

G

	Cell body	Neurites
C	+ + +	+
EXE	+ + +	+ + +
RA	+ + + +	+ +

Fig. 3 Representative epifluorescence microscope (100× magnification) images of actin (*left panels*) and tubulin (*right panels*) distribution in SH-SY5Y untreated cells (**a** and **d**) after treatment with exendin-4 (EXE) (**b** and **e**) or with RA (**c** and **f**). Semi-quantitative evaluation of the distribution and intensity of tubulin was performed by three different operators in at least ten fields (**g**)

Effect of exendin-4 on cofilin phosphorylation status

Cofilin is a member of the cofilin/actin depolymerizing factor family, which regulates actin filaments turnover and whose activation is regulated by its phosphorylation status. We performed a Western-blot analysis for the total and phosphorylated form of cofilin and we found that the phosphorylated (i.e., inactive) protein was significantly increased after 24 h of exendin-4 treatment, indicating that actin polymerization is paralleled by the inhibition of the activity of cofilin (Fig. 4a, b). Cofilin is also involved in

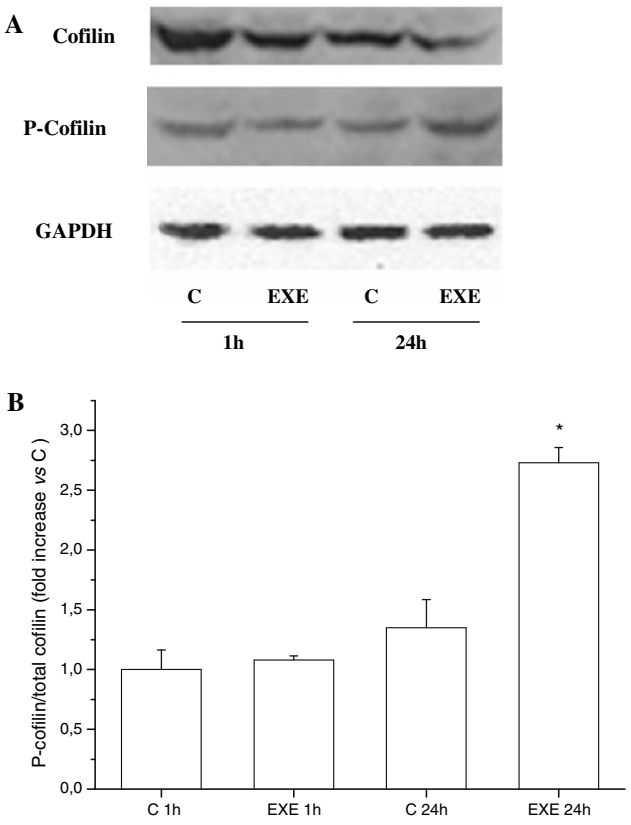

Fig. 4 **a** Western-blot representative experiment for the expression of cofilin, phosphorylated (P)-cofilin, and GAPDH proteins, detected in SH-SY5Y cells after 1- or 24-h treatment with exendin-4 (EXE). **b** Densitometric analysis of the P-cofilin/cofilin ratio. * = $p < 0.05$ versus control untreated cells (C), one-way ANOVA test

apoptosis induction, and we reasoned that its inactivation induced by exendin-4 might play a role in the previously described neuroprotective effects of this molecule [39, 40]. In order to determine whether these effects can be also observed in SH-SY5Y cells, viability assays were performed in cells exposed to oxidative stress. Treatment with 20 and 50 μM H_2O_2 significantly reduced cell viability. Noteworthy, overnight pre-incubation with exendin-4 protected SH-SY5Y cells from death, as demonstrated by both MTS (Fig. 5a) and Trypan Blue dye exclusion test (Fig. 5b). In addition, apoptosis evaluation was performed by TUNEL assay. As shown in Fig. 5c, the proportion of apoptotic cells was significantly greater in the H_2O_2 group than in the normal control group. However, pre-treatment with exendin-4 significantly counteracted H_2O_2-induced apoptosis. These results extend the neuroprotective actions of exendin-4 also in a human neuronal cell model.

Effects of exendin-4 and RA on the membrane passive properties of SH-SY5Y cells

The resting membrane potential (RMP), evaluated in current-clamp mode in physiological bath solution, was more depolarized in RA-treated cells (Fig. 6a). The membrane capacitance (C_m), as an estimate of cell-surface area, quantified in voltage-clamp mode, showed a significant increase in both exendin-4- and RA-treated cells (Fig. 6b). The specific resting membrane conductance (G_m/C_m), decreased in exendin-4-treated cells but showed insignificant increase in RA-treated cells (Fig. 6c). Thus, both exendin-4 and RA facilitated the growth of SH-SY5Y cells but with different actions, since exendin-4 reduced G_m/C_m and maintained its RMP whereas the contrary was observed in RA-treated cells.

Effects of exendin-4 and RA on the current density of stretch-activated channel, I_{SAC}/C_m in SH-SY5Y

As shown previously, we observed that exendin-4 treatment dramatically increased F-actin accumulation (Fig. 3b), whereas RA induced a weaker modification in actin polymerization (Fig. 3c). Considering that it was reported that actin polymerization and its contractile status increase the plasma membrane stiffness [41] and, in turn, increase the I_{SAC}/C_m [32] we evaluated this latter parameter to assess its relation to the different F-actin appearance in exendin-4 and RA-treated cells. The results clearly indicate that exendin-4 dramatically increased I_{SAC}/C_m whereas the potentiating effect of RA was significantly smaller respect to control (control 2.1 ± 0.25, exendin-4 12.2 ± 2.5, RA 2.8 ± 0.75; $p < 0.005$ and $p < 0.05$, respectively, compared to control). Experiments with $GdCl_3$, a well-known SAC blocker, confirmed that the recorded currents essentially flowed through SACs

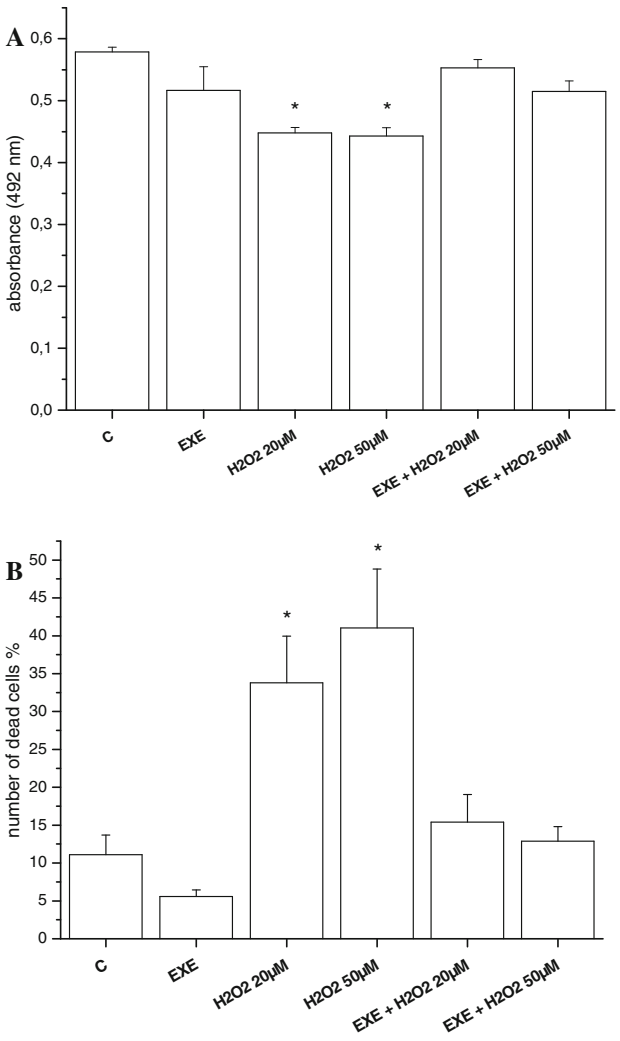

C

Sample	Apoptosis %
C	2.1 ± 0.26
EXE	2.7 ± 0.19
H_2O_2	9.8 ± 0.87*
EXE+H_2O_2	2.8 ± 0.28

Fig. 5 Effect of exendin-4 (EXE) pre-incubation on the viability of SH-SY5Y cells treated with H_2O_2 (20 and 50 μM) as assessed by MTS (**a**) and Trypan Blue dye exclusion (**b**) assays. Data are reported as mean ± SE. * = $p < 0.05$ versus control cells (C). **c** Number of TUNEL-positive cells/100 cells (mean ± SE of at least ten fields), detected in SH-SY5Y cells after H_2O_2 administration, with or without pre-treatment with exendin-4. * = $p < 0.05$ vs. control cells (C), one-way ANOVA test

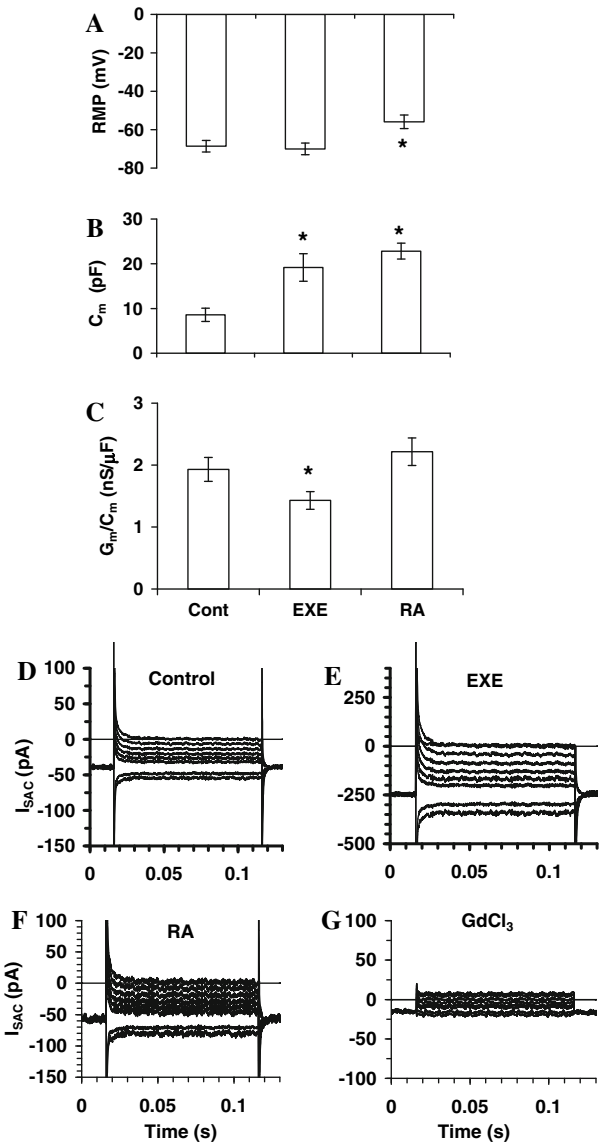

Fig. 6 Effects of exendin-4 (EXE) and RA on resting membrane potential and membrane passive properties of SH-SY5Y (**a**–**c**). Data recorded in physiological solution in control condition (Cont) and in exendin-4- (EXE) and RA-treated cells. **a** Resting membrane potential, RMP; **b** membrane capacitance, Cm; and **c** membrane normalized conductance, Gm/Cm. * $p < 0.05$ versus control vales. In each experimental condition, data from 25–29 cells are as mean ± ESM. Effects of exendin-4 and RA on ISAC in SH-SY5Y(*D*-*G*). Representative ISAC time course evoked by a pulse protocol 100 ms long, applied from −60 mV ranging from −80 to 0 mV in 10-mV increments. **d** Control cell; **e** exendin-4 dramatically increased ISAC/Cm whereas the potentiating effect of RA was significantly smaller (**f**) compared to control. **g** The addition of the SAC blocker $GdCl_3$, minimized the ionic currents confirming its origin through SACs

(Fig. 6g). In conclusion, the noticeable increase of F-actin accumulation in exendin-4-treated cells is paralleled by a strong increase of I_{SAC}/C_m, whereas RA induced a weaker action on F-actin accumulation as well as on I_{SAC}/C_m.

Effects of exendin-4 and RA on the electrophysiological properties of voltage-dependent ion channels in SH-SY5Y

Based on previous evidence indicating a positive effect of RA on neuron differentiation [33, 42–44], the effects on the electrophysiological properties of exendin-4 on SH-SY5Y cells were assessed and compared with those of RA. In 20-mM TEA solution, untreated cells exhibited I_{Na}, as shown in a typical experiment displayed in Fig. 7a. The voltage threshold of I_{Na} was about −60 mV. The treatment with exendin-4 definitively increased I_{Na} amplitude and this was more consistent in RA-treated cells (Fig. 7b, c). The normalized I–V plot determined at the current peak related to all the cells investigated is shown in Fig. 7d. The maximal current amplitude was recorded at -15 ± 5 mV in control cells, but it was at -20 ± 5 mV in exendin-4- and RA-treated cells (Fig. 7d). The Boltzmann parameters of the activation and inactivation curves underwent changes due to exendin-4 and RA treatment (Fig. 7e). The maximal current to peak and G_{Na} were increased to a similar extent with respect to control denoting that the current density increase was prevalently due to an augment of the channel conductance. The half voltage activation and inactivation parameters, V_a and V_i, were negatively shifted, respectively, about 5 and 3 mV (exendin-4) and 7 and 4 mV (RA) compared to the control. Moreover, the treatments did not affect the k_a values whereas k_i decreased (Fig. 7e; Table 1). In conclusion, exendin-4 and RA increased the I_{Na} availability by inducing a slight but significant voltage shift of V_a and V_i and by increasing the expression and/or conductance of the Na^+ channels.

To evaluate the presence of functional Ca^{2+} channels, we used TEA–Ca^{2+} bath solution (Fig. 8). In SH-SY5Y cells, Ca^{2+} channel currents consisted of two major components: (1) an inward transient and low-voltage-activated current (T-type Ca^{2+} current, I_{Ca},T) that was recorded from −50 mV, and (2) a high-voltage-activated and slow inactivating current (IHVA). The latter was recognized from −40 mV as a slower decaying current superimposed on the transient I_{Ca},T. Activation and inactivation Boltzmann curves of these two currents agree with T- and HVA-type of Ca^{2+} channels (Fig. 8h, i). This was confirmed by using Cd^{2+} and nifedipine, since none of them affected T-type current (Fig. 8d). Instead, HVA-type was blocked by Cd^{2+} but not completely by nifedipine, since a small size (about the 10% respect to control) and slow decaying current was still observed in nifedipine-treated cells. Accordingly, HVA currents prevalently consist of nifedipine-sensitive L-type and a small fraction of other Ca^{2+} currents such as N, P, Q, and R-types (Fig. 8d). The treatment with exendin-4 and RA definitely increased $I_{Ca,T}$, and $I_{Ca,L}$, amplitude (Fig. 8a–c) and this was consistently observed in all the experiments.

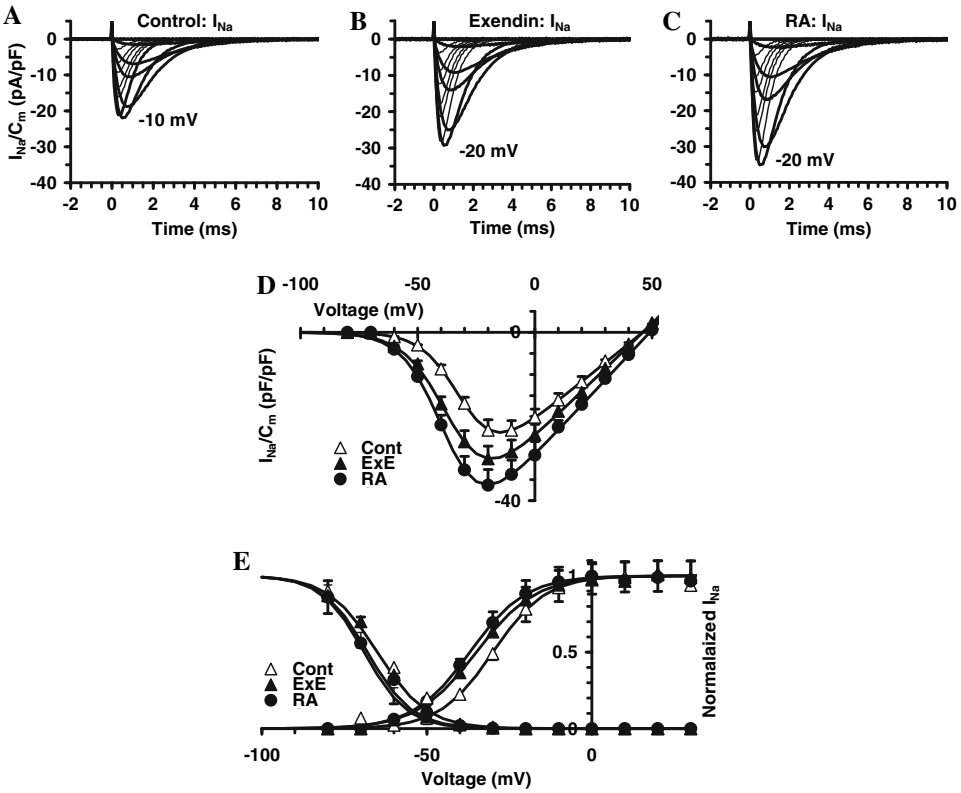

Fig. 7 Effects of exendin-4 (EXE) and RA on voltage-dependent Na+ channels in SH-SY5Y. **a** Typical I_{Na} traces recorded in 20-mM TEA solution in the presence of nifedipine (10 μM, evoked by a pulse protocol applied from an HP of −80 mV with 1-s step pulses ranging from –70 to 50 mV in 10-mV steps. The voltage threshold of I_{Na} was at −50 mV. **b** The treatment with exendin-4 increased I_{Na} amplitude and this was more consistent in RA-treated cells (**c**). In **a**–**c**, the voltage that elicited the maximal I_{Na} is indicated. **d** Normalized I–V plot determined at the current peak related to all the cells investigated. Superimposed on the data are Boltzmann fit curves (Eq. 1). **e** Normalized I_{Na} activation and inactivation data in control SH-SY5Y and under exendin-4 or RA treatment with superimposed the related Boltzmann fit; the Boltzmann curves for activation are obtained from fits in **c**. The related Boltzmann parameters are reported in Table 1. In each experimental condition data are from 26 to 43 cells

Table 1 Effect of EXE and RA treatment on Boltzmann parameters of activation and inactivation curves for I_{Na} and T- and L-type Ca^{2+} current in SH-SY5Y cells

Currents Param	I_{Na} Cont	I_{Na} EXE	I_{Na} RA	$I_{Ca,T}$ Cont	$I_{Ca,T}$ EXE	$I_{Ca,T}$ RA	$I_{Ca,L}$ Cont	$I_{Ca,L}$ EXE	$I_{Ca,L}$ RA
$I_p/I_{p,cont}$	1 ± 0.1	1.3 ± 0.2*	1.7 ± 0.2**	1 ± 0.1	1.2 ± 0.1*	1.2 ± 0.1*	1	1.7 ± 0.2**,[b]	1.9 ± 0.2**,[b]
G/G_{cont}	1 ± 0.1	1.2 ± 0.1*	1.3 ± 0.1*	1 ± 0.1	1.3 ± 0.1*	1.4 ± 0.1**,[a]	1 ± 0.1	1.8 ± 0.2**,[b]	2.2 ± 0.2**,[a,b]
V_a (mV)	−30 ± 2	−35 ± 2*	−37 ± 2*,[a]	−35 ± 2	−37 ± 2	−41 ± 3*,[a]	−18 ± 1	−22 ± 1*	−25 ± 2*,[a]
k_a (mV)	8 ± 0.3	9 ± 0.5	8 ± 1	5.7 ± 0.6	5.5 ± 0.4	5.4 ± 0.5	7.4 ± 0.3	7 ± 0.4	6.4 ± 0.5*,[a]
V_i (mV)	−65 ± 2	−68 ± 2*	−69 ± 3*	−65 ± 2	−70 ± 2*	−72 ± 2**	−50 ± 2	−55 ± 2*	−57 ± 2**,[a]
k_i (mV)	7.5 ± 0.3	6.5 ± 0.3*	6.6 ± 0.4*	4.5 ± 0.2	4.2 ± 0.3	4 ± 0.2*	7.5 ± 0.4	6.5 ± 0.4*	6.6 ± 0.4*

* and ** $p < 0.05$ and <0.01 versus the corresponding control

[a] $p < 0.05$ RA versus EXE

[b] $p < 0.05$ $I_{Ca,L}$ versus $I_{Ca,T}$ and I_{Na}. $I_p/_{p,cont}$ and G/G_{cont} are, respectively, the rate of peak currents and conductance in treated respect to control cells. For each current type, $I_p/I_{p,cont}$ are rates related to the respective control

The normalized I–V plots and the related normalized Boltzmann curve related to T- and L-type current are shown in Fig. 8h, i. Again, similar changes to those observed for I_{Na} were induced by exendin-4 and RA in Ca^{2+} currents, such as an increase in $G_{Ca,T}$ and $G_{Ca,L}$, a shift towards more negative potential of activation and inactivation V_a and V_i and a decrease of k_a and k_i. Notably, both the increase of the maximal current amplitude and the conductance of T- and L-type Ca^{2+} currents were greater than those of I_{Na}, and the highest increases were those related to L-type Ca^{2+} current.

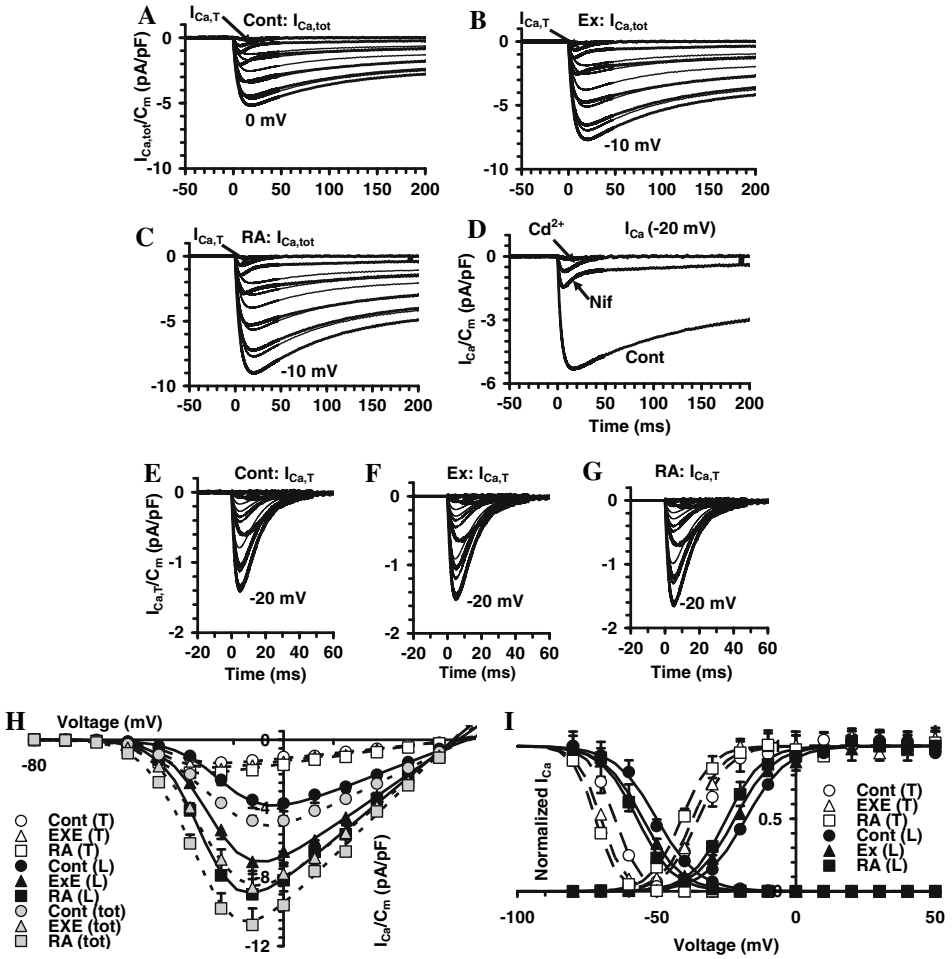

Fig. 8 Effects of exendin-4 (EXE) and RA on voltage-dependent Ca^{2+} channels in SH-SY5Y. Inward Ca^{2+} currents in SH-SY5Y. Representative ICa traces recorded in TEA-Ca^{2+} solution with TTX (1 μM) added obtained from SH-SY5Y in a control cell (**a**) and in exendin-4 (**b**) or RA (**c**)-treated cells. Current traces elicited from an HP of −80 mV by depolarizing steps from −70 to 50 mV in 10-mV increments are shown. $I_{Ca,tot}$ consisted of two major components. The traces at −50 mV clearly show the presence of a fast-activating and inactivating transient T-type Ca^{2+} current, $I_{Ca,T}$ (indicated by an *arrow* in the −50 mV trace) from −40 mV a high-voltage-activated and slow inactivating current (ICa,HVA), was recognized as a slower decaying current superimposed on the transient $I_{Ca,T}$. **d** Ca^{2+} currents elicited by a voltage step at −20 mV without (Cont) and in the presence of nifedipine (10 μM). **e–g** $I_{Ca,T}$ recorded at a holding potential of –50 mV that inactivate most $I_{Ca,HVA}$. **h** Normalized I–V plots determined at the current peaks in control and under exendin-4 or RA treatment. The total (tot) Ca^{2+} currents data with superimposed curves that are the best fit as a sum of two Boltzmann functions; *open symbols* represent data of $I_{Ca,T}$ obtained in the presence of nifedipine with superimposed curves that are the best fit of one Boltzmann function. **i** Normalized activation and inactivation data for T- and L-type Ca^{2+} current in control and under exendin-4 or RA treatment which superimposed the related Boltzmann fit; data and Boltzmann curves for activation are obtained from fits in **h**. The related Boltzmann parameters are reported in Table 1. In each experimental condition, data are from 22 to 27 cells

Lastly, some Boltzmann parameters were more affected by RA than by exendin-4 (Table 1).

Discussion

Our goal in this series of experiments was to study the properties of exendin-4 in terms of neuronal differentiation, using a human cell model (i.e., SH-SY5Y cells), which represents a recognized in vitro system for the assessment of neuronal differentiation [26, 27].

Since the GLP1-R is primarily coupled to the adenylate cyclase pathway via activation of Gs proteins, we have measured intracellular cAMP levels after exendin-4 treatment in our cell model, demonstrating that the receptor is functionally active. Differentiating properties of exendin-4 were previously observed for PC12 cells, in which biochemical changes were also found [25]. Here we compared the effects of exendin-4 to induce neurite extension in SH-SY5Y cells by using RA as a positive control. We found that exendin-4 is able to induce differentiation affecting the number of neurites present in the cells. Conversely, RA

appeared to be more effective in increasing the length of existing neurites. It is widely accepted that members of the Rho GTPase family are key regulators of actin dynamics and neuronal development [34]. The molecular analysis of the expression of Rho A and ROCK1 showed that exendin-4 treatment, as well as RA-treatment, significantly reduced the expression of both genes. Rho activation is generally associated with inhibition of neurite initiation and with retraction [45] and ROCK has been shown to mediate Rho actions by arresting cells in a round state or inducing neurite retraction [34]. Conversely, inactivation of Rho A/ROCK signaling pathway has been reported to induce neurite initiation and outgrowth [46]. Thus, our molecular data are in keeping with the morphological changes that we observed upon exendin-4 exposure. With regard to the possible mechanisms underlying the differentiating effects of exendin-4 in SH-SY5Y cells, we found that the PI3-K pathway is involved, whereas the MAPK/ERK pathway does not appear to play a role, as assessed by using the specific inhibitors LY294002 and U0126, respectively. Admittedly, this issue is worth further future investigation, in order to fully elucidate all the possible pathways that are involved.

The initial stages of neuritogenesis are regulated by mechanisms that involve reorganization of both microtubules and actin microfilaments [47]. Data published in the literature demonstrated that the initial rapid outgrowth phases of neuritogenesis are sensitive to the intracellular delivery of anti-tubulin antisera [48], thus suggesting that microtubules play important roles in neuronal morphogenesis. Our data, obtained by immunofluorescence microscopy, showed that exendin-4 treatment is effective in inducing multiple cytoskeletal rearrangements that result in neurite-like protrusions. By analyzing the expression of cytoskeletal components, we found that upon exendin-4 exposure, actin is strongly expressed and reorganized in stress fibers and cone-like structures, whereas this pattern is less evident both in control and in RA-treated cells. The effects observed in cells treated with exendin-4 or RA could reflect a different stage of neuronal differentiation. During early stages of neuritogenesis actin is polymerized from globular (G)-actin monomers to generate F-actin cones [49]. Our data clearly show the presence of visible actin-rich protrusions that could represent an initial phase of neuritogenesis. In keeping with these results, the membrane passive properties on the cell-surface area, estimated by measuring the membrane capacitance, showed a significant increase, indicating that the protrusions require the addition of new membrane surface. Moreover, the electrophysiological experiments confirmed that the noticeable increase of F-actin polymerization in exendin-4-treated cells was paralleled by a strong enhancement of the mechanical-sensitivity by increasing $I_{SAC,}$ thus allowing additional source of Ca^{2+} entry useful for differentiation and for the Ca^{2+}-dependent soma and neurites growth [50, 51]. Finally, exendin-4 treatment also improved the availability of voltage-activated I_{Na} and $I_{CaT,}$ and to a higher extent $I_{Ca,L}$: the changes of their activation and inactivation Boltzmann parameters are further indexes of neuronal differentiation towards more mature cells. Altogether, these findings suggest that exendin-4 acts as a neuronal plasticity-promoting agent. A role of GLP-1 in regulating neuronal differentiation has recently been investigated by Fisher et al. [52] who hypothesized that postnatal retinal neurogenesis is regulated by glucagon/GLP-1 and insulin, where the former might stimulate retinal progenitors to undergo differentiation.

Interestingly, we found that exendin-4 determined an increase of the amount of the phosphorylated form of cofilin. This protein is involved in actin filaments turnover by severing existing F-actin [53]. Furthermore, it has also been reported to have a role in apoptosis induction; in fact, it rapidly translocates to mitochondria upon exposure to apoptosis-inducing agents, thus allowing cell death to occur [40]. Both actin-severing and apoptosis-inducing activities are negatively regulated by phosphorylation [39]. Similarly to cofilin, the actin cytoskeleton itself, besides its involvement in neurite outgrowth, plays a crucial role in regulating cell responses to apoptotic signals [54–57].

Previous studies have indicated that exendin-4 possesses neuroprotective properties [22–24]. Accordingly, here we found that exendin-4 effectively counteracted H_2O_2-induced toxicity, as assessed by both MTS and Trypan Blue assays, and prevented apoptosis also in SH-SY5Y cells. Oxidative stress-induced cell death plays a critical role for instance in the pathogenesis of neurodegenerative diseases such as Alzheimer's disease (AD) and is intimately linked to aging. Accordingly, Perry and Greig suggested that GLP-1 and its analogs could be considered as potential novel therapeutic targets for intervention in AD, as well as in other central and peripheral neurodegenerative conditions [25]. With regard to this point, the differentiating properties of exendin-4 might be an additional important issue in favor of a role of exendin-4 in the treatment of these diseases. In fact, it has been reported that some substances that possess neurite outgrowth promoting effects in vitro might be useful for the treatment of neurodegenerative diseases by affecting the reconstruction of the damaged neural network that is observed in these conditions [58–60].

Altogether, our study thoroughly investigated for the first time the differentiating effects of exendin-4 in human neuronal cells, as assessed by morphological, structural, and electrophysiological observations. Our findings also indicated that cofilin might be a common key factor involved in the differentiating as well as in the

neuroprotective effects of this molecule. Since neuropathy represents one of the most debilitating complications of diabetes, these effects could have a clinical impact in patients taking this medication. This hypothesis is supported by the existence of ongoing clinical trials aiming to assess the effect of exenatide in the nervous system of diabetic patients (NCT00855439, NCT00747968; www.clinicaltrials.gov). Furthermore, our original data are in agreement with previous observations regarding a potential favorable effect of GLP-1 analogs for the treatment of different neuropathies such as AD [25].

Acknowledgments This study was supported by a grant from Ente Cassa di Risparmio di Firenze.

References

1. Zhou J, Pineyro MA, Wang X, Doyle ME, Egan JM (2002) Exendin-4 differentiation of a human pancreatic duct cell line into endocrine cells: involvement of PDX-1 and HNF3beta transcription factors. J Cell Physiol 192:304–314
2. Ugleholdt R, Zhu X, Deacon CF, Ørskov C, Steiner DF, Holst JJ (2004) Impaired intestinal proglucagon processing in mice lacking prohormone convertase 1. Endocrinology 145:1349–1355
3. Doyle ME, Egan JM (2007) Mechanisms of action of glucagon-like peptide 1 in the pancreas. Pharmacol Ther 113:546–593
4. Jang HJ, Kokrashvili Z, Theodorakis MJ (2007) Gut-expressed gustducin and taste receptors regulate secretion of glucagon-like peptide-1. Proc Natl Acad Sci USA 104:15069–15074
5. Willms B, Werner J, Holst JJ, Orskov C, Creutzfeldt W, Nauck MA (1996) Gastric emptying, glucose responses, and insulin secretion after a liquid test meal: effects of exogenous glucagon-like peptide-1 (GLP-1)-(7–36) amide in type 2 (noninsulin-dependent) diabetic patients. J Clin Endocrinol Metab 81:327–332
6. Komatsu R, Matsuyama T, Namba M, Watanabe N, Itoh H, Kono N, Tarui S (1989) Glucagonostatic and insulinotropic action of glucagons-like peptide I-(7–36)-amide. Diabetes 38:902–905
7. Estall JL, Drucker DJ (2006) Glucagon and glucagon-like peptide receptors as drug targets. Curr Pharm Des 12:1731–1750
8. Kolterman OG, Kim DD, Shen L, Ruggles JA, Nielsen LL, Fineman MS, Baron AD (2005) Pharmacokinetics, pharmacodynamics, and safety of exenatide in patients with type 2 diabetes mellitus. Am J Health Syst Pharm 62:173–181
9. Thorens B (1992) Expression cloning of the pancreatic beta cell receptor for the gluco-incretin hormone glucagon-like peptide 1. Proc Natl Acad Sci USA 89:8641–8645
10. Usdin TB, Mezey E, Button DC, Brownstein MJ, Bonner TI (1993) Gastric inhibitory polypeptide receptor, a member of the secretin-vasoactive intestinal peptide receptor family, is widely distributed in peripheral organs and the brain. Endocrinology 133:2861–2870
11. Moens K, Heimberg H, Flamez D, Huypens P, Quartier E, Ling Z, Pipeleers D, Gremlich S, Thorens B, Schuit F (1996) Expression and functional activity of glucagon, glucagon-like peptide I, and glucose-dependent insulinotropic peptide receptors in rat pancreatic islet cells. Diabetes 45:257–261
12. Ahren B (2004) GLP-1 and extra-islet effects. Horm Metab Res 36:842–845
13. Goke R, Larsen PJ, Mikkelsen JD, Sheikh SP (1995) Distribution of GLP-1 binding sites in the rat brain: evidence that exendin-4 is a ligand of brain GLP-1 binding sites. Eur J Neurosci 7:2294–2300
14. Tang-Christensen M, Larsen PJ, Göke R, Fink-Jensen A, Jessop DS, Møller M, Sheikh SP (1996) Central administration of GLP-1-(7–36) amide inhibits food and water intake in rats. Am J Physiol 271:R848–R856
15. Turton MD, O'Shea D, Gunn I, Beak SA, Edwards CM, Meeran K, Choi SJ, Taylor GM, Heath MM, Lambert PD, Wilding JP, Smith DM, Ghatei MA, Herbert J, Bloom SR (1996) A role for glucagon-like peptide-1 in the central regulation of feeding. Nature 379:69–72
16. Meeran K, O'Shea D, Edwards CM, Turton MD, Heath MM, Gunn I, Abusnana S, Rossi M, Small CJ, Goldstone AP, Taylor GM, Sunter D, Steere J, Choi SJ, Ghatei MA (1999) Bloom SR. Repeated intracerebroventricular administration of glucagon-like peptide-1-(7–36) amide or exendin-(9–39) alters body weight in the rat. Endocrinology 140:244–250
17. Baggio LL, Huang Q, Brown TJ, Drucker DJ (2004) Oxyntomodulin and glucagon-like peptide-1 differentially regulate murine food intake and energy expenditure. Gastroenterology 127:546–558
18. Abbott CR, Monteiro M, Small CJ, Sajedi A, Smith KL, Parkinson JR, Ghatei MA, Bloom SR (2005) The inhibitory effects of peripheral administration of peptide YY(3–36) and glucagon-like peptide-1 on food intake are attenuated by ablation of the vagal-brainstem-hypothalamic pathway. Brain Res 1044:127–131
19. Wei Y, Mojsov S (1995) Tissue-specific expression of the human receptor for glucagon-like peptide-I: brain, heart and pancreatic forms have the same deduced amino acid sequences. FEBS Lett 358:219–224
20. Perry T, Greig NH (2002) The glucagon-like peptides: a new genre in therapeutic targets for intervention in Alzheimer's disease. J Alzheimers Dis 4:487–496
21. During MJ, Cao L, Zuzga DS, Francis JS, Fitzsimons HL, Jiao X, Bland RJ, Klugmann M, Banks WA, Drucker DJ, Haile CN (2003) Glucagon-like peptide-1 receptor is involved in learning and neuroprotection. Nat Med 9:1173–1179
22. Perry T, Haughey NJ, Mattson MP, Egan JM, Greig NH (2002) Protection and reversal of excitotoxic neuronal damage by glucagon-like peptide-1 and exendin-4. J Pharmacol Exp Ther 302:881–888
23. Perry T, Lahiri DK, Sambamurti K, Chen D, Mattson MP, Egan JM, Greig NH (2003) Glucagon-like peptide-1 decreases endogenous amyloid-beta peptide (Abeta) levels and protects hippocampal neurons from death induced by Abeta and iron. J Neurosci Res 72:603–612
24. Li Y, Perry T, Kindy MS, Harvey BK, Tweedie D, Holloway HW, Powers K, Shen H, Egan JM, Sambamurti K, Brossi A, Lahiri DK, Mattson MP, Hoffer BJ, Wang Y, Greig NH (2009) GLP-1 receptor stimulation preserves primary cortical and dopaminergic neurons in cellular and rodent models of stroke and Parkinsonism. Proc Natl Acad Sci USA 106:1285–1290
25. Perry T, Lahiri DK, Chen D, Zhou J, Shaw KT, Egan JM, Greig NH (2002) A novel neurotrophic property of glucagon-like peptide 1: a promoter of nerve growth factor-mediated differentiation in PC12 cells. J Pharmacol Exp Ther 300:958–966
26. Påhlman S, Ruusala AI, Abrahamsson L, Mattsson ME, Esscher T (1984) Retinoic acid-induced differentiation of cultured human neuroblastoma cells: a comparison with phorbolester-induced differentiation. Cell Differ 14:135–144
27. Toselli M, Masetto S, Rossi P, Taglietti V (1991) Characterization of a voltage-dependent calcium current in the human neuroblastoma cell line SH-SY5Y during differentiation. Eur J Neurosci 3:514–522

28. Livak KJ, Schmittgen TD (2001) Analysis of relative gene expression data using real-time quantitative PCR and the 2(-delta delta C(T)) method. Methods 25:402–408
29. Benvenuti S, Luciani P, Vannelli GB, Gelmini S, Franceschi E, Serio M, Peri A (2005) Estrogen and selective estrogen receptor modulators exert neuroprotective effects and stimulate the expression of selective Alzheimer's disease indicator-1: a recently discovered antiapoptotic gene, in human neuroblast long-term cell cultures. J Clin Endocrinol Metab 90:1775–1782
30. Luciani P, Ferruzzi P, Arnaldi G, Crescioli C, Benvenuti S, Nesi G, Valeri A, Greeve I, Serio M, Mannelli M, Peri A (2004) Expression of the novel adrenocorticotropin-responsive gene selective Alzheimer's disease indicator-1 in the normal adrenal cortex and in adrenocortical adenomas and carcinomas. J Clin Endocrinol Metab 89:1332–1339
31. Formigli L, Francini F, Tani A, Squecco R, Nosi D, Polidori L, Nistri S, Chiappino L, Cesati V, Pacini A, Perna AM, Orlandini GE, Zecchi Orlandini S, Bani D (2005) Morphofunctional integration between skeletal myoblasts and adult cardiomyocytes in coculture is favored by direct cell-cell contacts and relaxin treatment. Am J Physiol Cell Physiol 288:795–804
32. Formigli L, Sassoli C, Squecco R, Bini F, Martinesi M, Chellini F, Luciani G, Sbrana F, Zecchi-Orlandini S, Francini F, Meacci E (2009) Regulation of transient receptor potential canonical channel 1 (TRPC1) by sphingosine 1-phosphate in C2C12 myoblasts and its relevance for a role of mechanotransduction in skeletal muscle differentiation. J Cell Sci 122:1322–1333
33. Abemayor E, Sidell N (1989) Human neuroblastoma cell lines as models for the in vitro study of neoplastic and neuronal cell differentiation. Environ Health Perspect 80:3–15
34. Govek EE, Newey SE, Van Aelst L (2005) The role of the Rho GTPases in neuronal development. Genes Dev 19:1–49
35. Kim W, Egan JM (2008) The role of incretins in glucose homeostasis and diabetes treatment. Pharmacol Rev 60:470–512
36. Liu J, Zheng X, Yin F, Hu Y, Guo L, Deng X, Chen G, Jiajia J, Zhang H (2006) Neurotrophic property of geniposide for inducing the neuronal differentiation of PC12 cells. Int J Dev Neurosci 24:419–424
37. Nakaso K, Ito S, Nakashima K (2008) Caffeine activates the PI3 K/Akt pathway and prevents apoptotic cell death in a Parkinson's disease model of SH-SY5Y cells. Neurosci Lett 432:146–150
38. Miloso M, Villa D, Crimi M, Galbiati S, Donzelli E, Nicolini G, Tredici G (2004) Retinoic acid-induced neuritogenesis of human neuroblastoma SH-SY5Y cells is ERK independent and PKC dependent. J Neurosci Res 75:241–252
39. Arber S, Barbayannis FA, Hanser H, Schneider C, Stanyon CA, Bernard O, Caroni P (1998) Regulation of actin dynamics through phosphorylation of cofilin by LIM-kinase. Nature 393:805–809
40. Chua BT, Volbracht C, Tan KO, Li R, Yu VC, Li P (2003) Mitochondrial translocation of cofilin is an early step in apoptosis induction. Nat Cell Biol 5:1083–1089
41. Sbrana F, Sassoli C, Meacci E, Nosi D, Squecco R, Paternostro F, Tiribilli B, Zecchi-Orlandini S, Francini F, Formigli L (2008) Role for stress fiber contraction in surface tension development and stretch-activated channel regulation in C2C12 myoblasts. Am J Physiol Cell Physiol 295:C160–C172
42. Anghileri E, Marconi S, Pignatelli A, Cifelli P, Galié M, Sbarbati A, Krampera M, Belluzzi O, Bonetti (2008) Neuronal differentiation potential of human adipose-derived mesenchymal stem cells. Stem Cells Dev 17:909–916
43. Erceg S, Laínez S, Ronaghi M, Stojkovic P, Pérez-Aragó MA, Moreno-Manzano V, Moreno-Palanques R, Planells-Cases R, Stojkovic M (2008) Differentiation of human embryonic stem cells to regional specific neural precursors in chemically defined medium conditions. PLoS One 3:e2122
44. Martinez-Monedero R, Yi E, Oshima K, Glowatzki E, Edge AS (2008) Differentiation of inner ear stem cells to functional sensory neurons. Dev Neurobiol 68:669–684
45. Yamaguchi Y, Katoh H, Yasui H, Mori K, Negishi M (2001) RhoA inhibits the nerve growth factor-induced Rac1 activation through Rho-associated kinase-dependent pathway. J Biol Chem 276:18977–18983
46. Bito H, Furuyashiki T, Ishihara H, Shibasaki Y, Ohashi K, Mizuno K, Maekawa M, Ishizaki T, Narumiya S (2000) A critical role for a Rho-associated kinase, p160ROCK, in determining axon outgrowth in mammalian CNS neurons. Neuron 26:431–441
47. Dehmelt L, Smart FM, Ozer RS, Halpain S (2003) The role of microtubule-associated protein 2c in the reorganization of microtubules and lamellipodia during neurite initiation. J Neurosci 23:9479–9490
48. Shea TB, Beermann ML (1994) Respective roles of neurofilaments, microtubules, MAP1B, and Tau in neurite outgrowth and stabilization. Mol Biol Cell 5:863–875
49. Berneistein BW, Bamburg JR (1992) Actin in emerging neurites is recruited from a monomer pool. Mol Neurobiol 6:95–106
50. Henley J, Poo MM (2004) Guiding neuronal growth cones using Ca21 signals. Trends Cell Biol 14:320–330
51. D'Ascenzo M, Piacentini R, Casalbore P, Budoni M, Pallini R, Azzena GB, Grassi C (2006) Role of L-type Ca2 + channels in neural stem progenitor cell differentiation. Eur J Neurosci 23:935–944
52. Fischer AJ, Omar G, Walton NA, Verrill TA, Unson CG (2005) Glucagon-expressing neurons within the retina regulate the proliferation of neural progenitors in the circumferential marginal zone of the avian eye. J Neurosci 25:10157–10166
53. Ichetovkin I, Grant W, Condeelis J (2002) Cofilin produces newly polymerized actin filaments that are preferred for dendritic nucleation by the Arp2/3 complex. Curr Biol 12:79–84
54. Rosen K, Rak J, Leung T, Dean NM, Kerbel RS, Filmus J (2000) Activated Ras prevents downregulation of Bcl-X(L) triggered by detachment from the extracellular matrix. A mechanism of Ras-induced resistance to anoikis in intestinal epithelial cells. J Cell Biol 149:447–456
55. Posey SC, Bierer BE (1999) Actin stabilization by jasplakinolide enhances apoptosis induced by cytokine deprivation. J Biol Chem 274:4259–4265
56. Parlato S, Giammarioli AM, Logozzi M, Lozupone F, Matarrese P, Luciani F, Falchi M, Malorni W, Fais S (2000) CD95 (APO-1/Fas) linkage to the actin cytoskeleton through ezrin in human T lymphocytes: a novel regulatory mechanism of the CD95 apoptotic pathway. EMBO J 19:5123–5134
57. Yang EJ, Yoon JH, Min DS, Chung KC (2004) LIM kinase 1 activates cAMP-responsive element-binding protein during the neuronal differentiation of immortalized hippocampal progenitor cells. J Biol Chem 279:8903–8910
58. Gillespie LN (2003) Regulation of axonal growth and guidance by the neurotrophin family of neurotrophic factors. Clin Exp Pharmacol Physiol 30:724–733
59. O'Neill K, Chen S, Brinton RD (2004) Impact of the selective estrogen receptor modulator, raloxifene, on neuronal survival and outgrowth following toxic insults associated with aging and Alzheimer's disease. Exp Neurol 185:63–80
60. Tohda C, Matsumoto N, Zou K, Meselhy MR, Komatsu K (2004) Abeta(25–35)-induced memory impairment, axonal atrophy and synaptic loss are ameliorated by M1, a metabolite of protopanaxadiol-type saponins. Neuropsychopharmacology 29:860–868